Arboreal Lagrangian skeleta and Legendrian handlebodies

SAM SOTTILE, EHA SRIVASTAVA, JESSICA ZHANG

Abstract. Handlebody constructions using Weinstein handles offer a convenient method of studying symplectic manifolds. Alternatively, symplectic manifolds can be studied via their skeleton, which encodes much of the data of the entire manifold. In particular, arboreal Lagrangian skeleta have simple enough singularities so that the entire manifold can be recovered from just the skeleton itself. In this paper, we prove that the symplectic 4-manifold obtained by attaching a Weinstein 2-handle to a 0-handle along a Legendrian $(2, 2g + 1)$-torus knot is equivalent to the cotangent bundle of the genus g surface with $2g$ Lagrangian disks attached. In particular, the $2g$ Lagrangian disks constitute an arboreal Lagrangian skeleton for this manifold. In this work, we establish the handlebody diagrams for the two presentations of this manifold and prove they are equivalent using Legendrian Reidemeister moves and Weinstein handle-sliding/cancellation.

Contents

1. Introduction

It is important in geometry to be able to say, given two different presentations of seemingly different geometric objects, whether they are in fact the same or not. One direction—showing two things are different—depends on being able to find *invariants* of these objects which are always the same, no matter the presentation. Thus if two objects have different invariants, then we immediately know that they are in fact completely different. In the other direction—showing two things are in fact the same—depends on being able to *construct* an equivalence, whether via a series of set moves which are known to preserve the object, or via an explicit isomorphism.

Of course, this entire question depends a priori on a notion of "sameness." There are, in fact, many different notions of "sameness," or equivalence. In our case, we are concerned with *symplectic manifolds*, i.e., smooth manifolds with a symplectic structure. Two symplectic manifolds are then considered "the same," or *symplectomorphic*, if there is a bijective map from one to another which is smooth in both directions and which in some sense preserves the symplectic structure.

To be able to tell if two symplectic manifolds are different then depends on our ability to find and calculate various invariants of symplectic manifolds, i.e., various quantities which are preserved by symplectomorphism. Unfortunately, many invariants of symplectic geometry can be quite difficult

2010 *Mathematics Subject Classification.* Primary: 53D10. Secondary: 53D15, 57R17.

to calculate. However, if the symplectic manifold satisfies a slightly stronger condition that it is *Liouville*, then we can define a subset of the manifold called its *skeleton*. The skeleton is further called *arboreal* if all its singularities can be classified as arboreal, as introduced by D. Nadler in [4]. An arboreal skeleton uniquely determines the original manifold, so that understanding the manifold amounts to understanding its skeleton. Furthermore, arboreal singularities offer more convenient methods to define and compute sheaf-theoretic invariants of symplectic manifolds, which in turn yield information about the Fukaya category of the manifold. As such, it's important to how to find arboreal skeleta, and determine which manifolds even admit an arboreal skeleton in the first place.

In this paper, we examine a relatively simple class of symplectic 4-manifolds and determine an arboreal Lagrangian skeleton for them. Although arboreal Lagrangian skeleta help us determine when two manifolds are not symplectomorphic, we will show that these 4-manifolds are in fact equivalent to another class of symplectic 4-manifolds. In particular, we provide an explicit description of the arboreal skeleton for this second class of 4-manifolds, which in turn determines an arboreal skeleton for the original manifolds. We first provide the necessary background on handlebody decompositions and Kirby calculus in the smooth setting. These decompositions provide convenient descriptions of smooth manifolds, as well how these presentations may be manipulated. We then present the symplectic analogue of this theory and provide background on Weinstein handlebody constructions and diagrams. By determining the Weinstein handlebody diagram of a symplectic 4-manifold, we can determine if this 4-manifold is equivalent to another by relating the two handlebody diagrams via symplectic analogues of handle sliding and cancellation. After the relevant background information, we present the main results of this paper. We first establish the Weinstein handlebody diagrams for our manifolds of interest and prove a number of technical lemmas on manipulating these diagrams. Finally, we prove the equivalence of the symplectic 4-manifolds, establishing an arboreal Lagrangian skeleton.

2. Background

2.1. **Handle decompositions.** Let M be a smooth, compact n-manifold. Following the presentation given in [3], decompose its boundary ∂M as $\partial_+ M \coprod \partial_- M$, with appropriate orientations if M is oriented. Then we can obtain M from $\partial_- M$ by attaching *(n-dimensional) handles*. In particular, for $0 \leq k \leq n$, an *n-dimensional k-handle* h is a copy of $D^k \times D^{n-k}$, along with an attaching embedding $\varphi : \partial D^k \times D^{n-k} \to \partial M$. Every smooth, compact pair $(M, \partial_- M)$ admits a *handle decomposition*, that is, a way to obtain M by attaching handles to $I \times \partial_- M$, where $\partial_- M$ is identified with $\{0\} \times \partial_- M$. If M is equipped with a given handle decomposition and $\partial_- M = \emptyset$, then we call M a *handlebody*.

As in Figure 1 , we call $D^k \times \{0\}$ the *core* of the handle and $\{0\} \times D^{n-k}$ the *cocore*. We also call (the images of) $\partial D^k \times \{0\}$ and $\{0\} \times \partial D^{n-k}$ the *attaching sphere* and *belt sphere*, respectively.

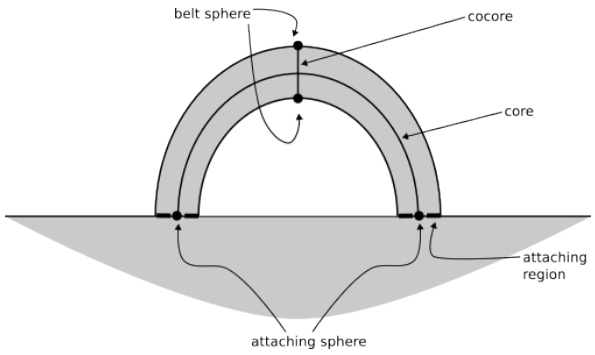

Figure 1. The anatomy of a handle

We are only interested in $M \cup_\varphi h$ up to diffeomorphism type, where $h = D^k \times D^{n-k}$ is a handle attached to M along φ. This turns out to depend only on the isotopy type of φ, which in turn depends only on a choice of knot $\varphi_0 : \partial D^k \times \{0\} = S^{k-1} \to \partial M$ and a *framing* of $\varphi_0(S^{k-1})$, i.e., a trivialization of the normal bundle $\nu\varphi_0(S^{k-1})$. In general, the set of isotopy classes of framings of S^{k-1} in ∂M is in bijection with $\pi_{k-1}(O(n-k))$. For example, since $\pi_0(O(n-1)) = \mathbb{Z}/2\mathbb{Z}$ for $n \geq 2$, we know that

there are only two framings for a 1-handle in dimension $n \geq 2$. If the original manifold was oriented, then there is in fact a unique such framing.

In general, handle decompositions can be obtained by Morse functions on the manifold. Since Morse functions exist generically, it follows that a given manifold generally admits many handle decompositions. Given any such handle decomposition, we can first standardize the order of handle attachment. In particular, a dimension argument implies that we can always attach handles in order of increasing index. (Handles of the same index can be attached in any order, or at the same time.)

Then any two handle decompositions, after ordering them as described above, can be related via some (finite) sequence of *handle creation/cancellation* and *handle sliding*.

For the first of these steps, consider Figure 2. The two manifolds are clearly diffeomorphic, but the

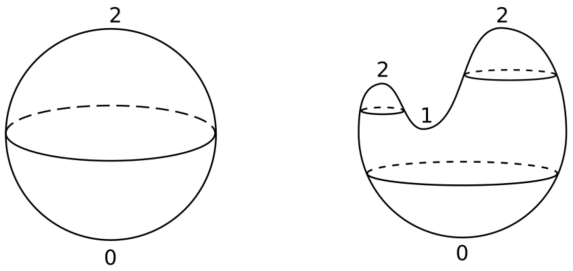

FIGURE 2. Handle creation/cancellation

handle decompositions are different. Indeed, to get the decomposition on the right from the one on the left requires a handle creation; conversely, to get the decomposition on the left from the one on the right requires a handle cancellation. In general, a $(k-1)$-handle h_{k-1} and a k-handle h_k can be canceled exactly when the attaching sphere of h_k and the belt sphere of h_{k-1} intersect transversely at a single point. (In Figure 2, note that the belt sphere of $h_{k-1} = h_1$ and the attaching sphere of $h_k = h_2$ are both S^0. Thus their intersection, which is clearly a single point, is necessarily transverse.)

Intuitively, handle sliding simply involves pushing one k-handle over another. In particular, if $0 < k < n$, then a handle slide corresponds to the isotopy given by pushing the attaching sphere A of one k-handle h over and across the core of another k-handle h'. This will push A through the belt sphere B of h'. Note that when A intersects B nontrivially, it does so at a single point. There are then two directions in which we can isotope the handles: One direction takes us back to our original decomposition; the other is the result of the handle slide.

Using some ideas from Morse theory, one can then show that any two handle decompositions (ordered by increasing index) can be obtained from each other by some sequence of these steps.

One advantage of handle decompositions is that they allow us to draw 4-dimensional objects in a relatively simple manner, called the *Kirby diagram*. In particular, to uniquely determine an oriented 4-manifold without boundary, it is enough data to give the set of attaching spheres and the framing for each handle.

First, we can always assume that there is a single 0-cell whose attaching sphere is $S^4 = \mathbb{R}^3 \cup \{\infty\}$. All further handles can be attached to this 0-cell (or to prior added handles). We can of course perturb these attachments to avoid ∞. Since we only care about the attaching regions, we can imagine drawing the manifold as a bunch of attaching spheres on $\mathbb{R}^3$, each with a specified framing.

However, as mentioned before, given a handle decomposition for an oriented 4-manifold, there is only one possible framing for each of its 1-handles. Thus we need not specify the framing for 1-handles. We also know that the framings for 2-handles correspond to elements of $\pi_1(O(2)) = \mathbb{Z}$, so we only need to write a number for 2-handles.

It turns out that it is actually enough to only draw k-handles for $k \leq 2$. That the 4-handles are determined is clear: Since the manifold was assumed not to have boundary, the attaching spheres of the 4-handles are necessarily the boundary components; there is only one possible framing. It is much more difficult to prove that the 3-handles are also determined, though we take it on faith here.

Hence we can effectively draw any 4-manifold by drawing pairs of S^2's (the attaching spheres for the 1-handles) and knots (the attaching spheres for the 2-handles). Note that we must label the knots with numbers, however, which correspond to the framing.

As an example, consider Figure 3. This shows a disk bundle over the torus. In the case $n = 0$, this

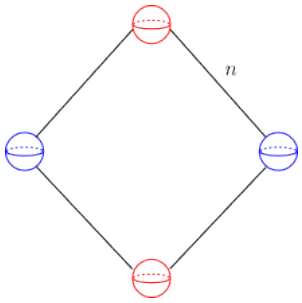

FIGURE 3. Kirby diagram of a D^2-bundle over T^2 with Euler number n

is simply the trivial bundle, which is also the cotangent bundle.

2.2. **Liouville and Weinstein manifolds.** Recall that a *symplectic form* on a smooth manifold M is a closed and nondegenerate 2-form. Given a manifold M and a symplectic form ω defined on M, we call the pair (M, ω) a *symplectic manifold*. A submanifold $X \subset M$ is a *Lagrangian submanifold* if $\omega_p|_{T_pY} \equiv 0$ at each $p \in Y$ and $\dim T_pY = \frac{1}{2}\dim T_pM$. A vector field V on a symplectic manifold (M, ω) is called a *Liouville vector field* if it satisfies the property

$$\mathcal{L}_V \omega = \omega.$$

If a symplectic manifold (M, ω) comes equipped with a Liouville vector field V transverse to the boundary ∂M, then V defines a contact structure on ∂M. In particular, there exists a 1-form $\alpha \in \Omega^1(\partial M)$ defining $\xi = \ker(\alpha)$ such that $\alpha \wedge d\alpha^{n-1} > 0$.

A symplectic manifold (M, ω) with a Liouville vector field V is a *Liouville manifold* if it can be decomposed into compact domains M_k such that $M = \bigcup_k M_k$ and V is outwardly transverse to the boundary of each M_k. The *skeleton* of such a Liouville manifold (M, ω, V) is

$$Skel(M, \omega, V) = \bigcup_{k=1}^{\infty} \bigcap_{t>0} V^{-t}(M_k).$$

Here, V^{-t} denotes the $-t$ flow of V, and M_k is a compact exhaustion of M as described above. In this setting, two symplectic manifolds with boundary such that the Liouville vector field of one manifold points outward along its boundary and the Liouville vector field of the other points inward along its boundary can be glued along their boundaries.

Note that the skeleton depends on a choice of Liouville vector field; thus a given symplectic manifold (M, ω) may have many skeleta.

This gives a way to systematically construct symplectic manifolds using handle decompositions. A $2n$-dimensional *Weinstein k-handle* H_k is defined as follows: Consider $\mathbb{R}^{2n}$ with coordinates $(x_1, y_1, \ldots, x_n, y_n)$, equipped with the standard symplectic form $\omega = \sum_{i=1}^n dx_i \wedge dy_i$ and Liouville vector field

$$V_k = \sum_{i=1}^{k} (-x_i \partial_{x_i} + 2y_i \partial_{y_i}) + \sum_{i=k+1}^{n} \left(\frac{1}{2} x_i \partial_{x_i} + \frac{1}{2} y_i \partial_{y_i} \right).$$

The k-handle is a subset $H_k \subset \mathbb{R}^{2n}$ diffeomorphic to $D^k \times D^{2n-k}$. The boundary of H_k decomposes into two parts, $\partial_- H_k$ and $\partial_+ H_k$, such that V_k points inward along $\partial_- H_k$ and outward along $\partial_+ H_k$. Thus, we can glue together Weinstein k-handles ($k \leq 2n$), resulting in a symplectic manifold. Such a manifold is called a *Weinstein domain*, and its cylindrical completion is a *Weinstein manifold*. It can be shown that a handlebody decomposition for a $2n$-dimensional Weinstein domain/manifold contains only k-handles for $k \leq n$. In particular, a Weinstein 4-manifold is built entirely of 0, 1, and 2-handles.

Before we continue on and briefly develop the material from Section 2.1 in the symplectic/Weinstein case, let us return to the topic of skeleta. The skeleton of a Liouville manifold encodes, in a certain

sense, much of the information of the original manifold. In particular, an arbitrarily small neighborhood of the skeleton completely recovers the Weinstein manifold itself. Furthermore, a nice enough skeleton allows us to in turn completely recover such a neighborhood. Thus studying a nice skeleton of a given Weinstein manifold, which is also generally of lower dimension than the original manifold, can make computations of certain invariants easier.

We have not yet explained what we mean by "nice enough." Certainly, it is enough for the skeleton to also a Lagrangian submanifold. This, however, is often not the case. Fortunately, we can generalize the class of skeleta that allows us to recover the original manifold to be that of *arboreal* Lagrangian skeleta.

For our purposes, an *arboreal skeleton* of (M, ω, V) is one such that each point of M has a neighborhood which looks like one of the three in Figure 4. In words, the manifold is one of the following three

FIGURE 4. Possible local models for an arboreal skeleton

possibilities at each point: Euclidean; $\mathbb{H} \times [0, 1]$, where $\mathbb{H}$ denotes the upper half-plane $\{(x, y) : y \geq 0\}$; or like two "fins." More or less, the singularities all arise from intersections with embedded disks.

2.3. **Weinstein handlebody diagrams and Kirby calculus.** Handlebody decompositions offer a convenient presentation of complicated manifolds in the smooth setting. The use of handlebody diagrams can simplify the process of computing invariants and determining equivalences between manifolds. An analogue of this in symplectic geometry is given by Weinstein's construction of symplectic handles, presented in [5]. In particular, Gompf developed a standard form for Weinstein handlebody diagrams in dimension 4, which fully characterize the Weinstein handlebody structure and can be manipulated by equivalence moves [2]. Weinstein handlebody diagrams in dimension 4 are simply front projections of Legendrian knots in $(\#^k(S^1 \times S^2), \xi_{std})$, which encode the Legendrian attaching spheres of the 2-handles in the boundary of the 1-handlebody. Notably, this means that manipulating the Legendrian attaching spheres via Legendrian Reidemeister moves results in a symplectomorphic handlebody diagram. To describe manipulations of these attaching spheres, we will usually refer to the relevant portion of the Legendrian knot as the "strand" that is being moved. In this section, we will review the basics of constructing Weinstein handlebody diagrams, with an emphasis on dimension 4.

To describe a Weinstein handlebody construction, we only need to describe how the handles are attached. For a connected Weinstein 4-manifold, we begin with a single 0-handle, which has boundary S^3. By implicitly taking there to be a point at infinity, we may depict the construction in $\mathbb{R}^3$. Then the attaching region of the attaching sphere $S^0 \times \{0\}$ of a 1-handle is drawn as a pair of 3-balls. In the Weinstein setting, the attaching sphere $S^1 \times \{0\}$ of a 2-handle is a Legendrian knot, which is represented by its front projection. In the smooth case, the 4-dimensional 2-handle attachment is determined by the isotopy class of the knot along with a framing. In the Weinstein case, the framing is actually predetermined by the contact structure. Therefore, it suffices to simply consider the front projections of the attaching spheres of the 2-handles. For example, the standard Gompf diagramfor the general genus g surface is shown in Figure 5 below. Since the front projection captures all the information about the attachment of a 2-handle, the Legendrian Reidemeister moves (shown in Figure 6 below) relate Weinstein diagrams in Gompf standard form.

There is also a symplectic analogue of handle slides and handle pair cancellations. As in the smooth case, two Weinstein handlebody diagrams are equivalent if they can be related by a sequence of Weinstein handle slides/cancellations. In the Weinstein setting, the isotopies must additionally be Legendrian. These moves are shown in Figure 7.

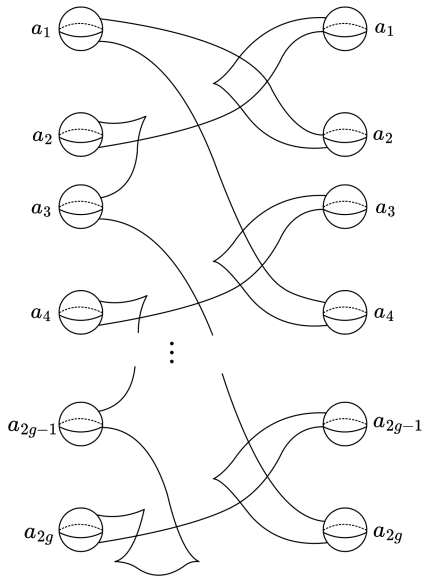

FIGURE 5. The Gompf diagram for the (cotangent bundle of the) genus g surface

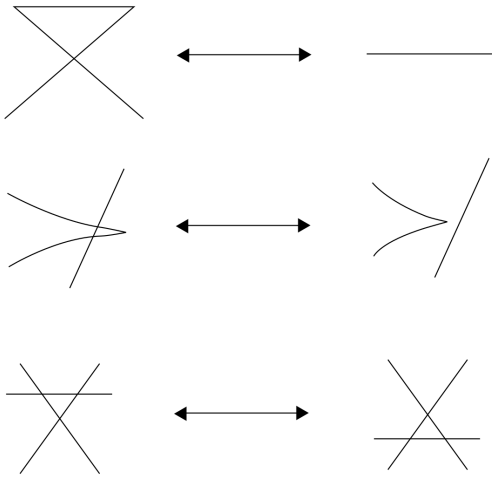

FIGURE 6. The three Legendrian Reidemeister moves

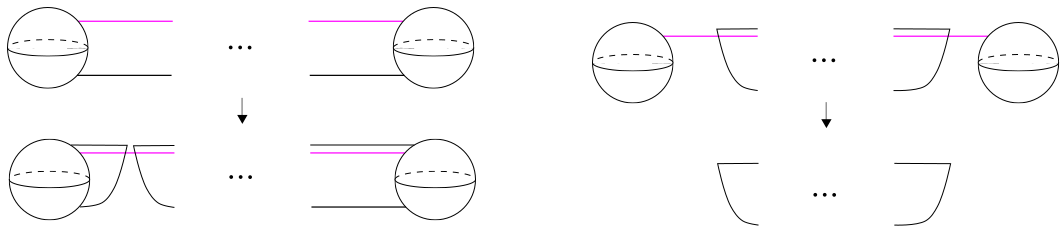

(A) Sliding the black handle over the pink handle (B) Canceling the pink handle with the 1-handle

FIGURE 7. Handle moves in Weinstein Kirby diagrams

In general, our goal in this paper will be to show certain Weinstein Kirby diagrams are equivalent. To do so, we show that we can obtain one from the other via a sequence of handle slides, handle cancellations, and Legendrian Reidemeister moves.

3. Results

Consider the Weinstein 4-manifold $M = X_n$ obtained by attaching a Weinstein 2-handle to a 0-handle along a Legendrian $(2, n)$-torus knot. Our goal was to find an arboreal Lagrangian skeleton for this manifold. To do so, we proved that M was equivalent to the 4-manifold by attaching the $4n$ Lagrangian 2-disks as shown in Figure 8 to the cotangent bundle of the genus g surface, Σ_g. Since

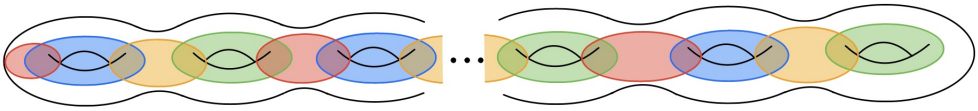

Figure 8. $T^*\Sigma_g$ with $4g$ embedded Lagrangian disks.

this manifold clearly has an arboreal skeleton, namely the surface depicted in Figure 8, it follows that this is in fact the arboreal skeleton of M, as desired.

3.1. Determining the Weinstein handlebody diagrams.

Because equivalence of Weinstein 4-manifolds can be shown by manipulating the corresponding Weinstein handlebody diagram, we first establish the handlebody diagram for $T^*\Sigma_g$ with the Lagrangian 2-disks attached.

Proposition 3.1. *The Weinstein handlebody diagram for $T^*\Sigma_g$ with $2g$ Lagrangian disks attached is given as in Figure 9.*

Proof. Consider the handlebody diagram of the cotangent bundle of the genus g surface, $T^*\Sigma_g$, drawn in Gompf standard form, as in Figure 5. The handlebody diagram of $T^*\Sigma_g$ consists of one 0-handle, $2g$ 1-handles, and one 2-handle attached along the indicated curve. As in the diagram, label the 1-handles from top to bottom as $a_1, a_2, \ldots, a_{2g-1}, a_{2g}$.

To motivate the general case, first consider the genus 1 and 2 cases, as pictured in Figure 10. When $g = 1$, the attaching sphere of the 2-handle intersects the 1-handles in the order a_1, a_2, a_1, a_2. Similarly, for $g = 2$, the attaching sphere of the 2-handle intersects the 1-handles in the order $a_1, a_4, a_3, a_4, a_3, a_2, a_1, a_2$. We can use a combination of Reidemeister moves to simplify the colored curves.

In general, suppose we know the order in which the 2-handle intersects the 1-handles in the genus $g-1$ case. Then to find the order in which the 2-handle intersects the 1-handles in the Gompf diagram for the genus g case, there are two possibilities we must consider:

(1) If g is even, take the sequence of intersections for the $g-1$ case and insert the sequence
$$a_{2g}, a_{2g-1}, a_{2g}, a_{2g-1}$$
after the first a_{2g-3}.
(2) If g is odd, take the sequence of intersections for the $g-1$ case and insert the sequence
$$a_{2g-1}, a_{2g}, a_{2g-1}, a_{2g}$$
after the second a_{2g-2}.

Recall that we may represent the genus g surface as a $4g$-gon with sides appropriately identified. With the above order of intersections in mind, we can identify the curves comprising the skeleton on the 4-gon and draw in the Legendrian lifts to $T^*\Sigma_2$ on the Gompf diagram of $T^*\Sigma_2$. Again, we start by considering the genus 1 and 2 cases. For the genus 1 case, the skeleton consists of a disk bounded by a meridian and a disk bounded by a longitude. Figure 11 displays the disks on the genus 1 surface and the corresponding boundary curves on the representative polygon. As in [1] the Legendrian lifts of the boundary curves to $T^*\Sigma_1$ can be drawn on the Gompf diagram in Figure 12. In particular, these lifts are drawn by following the attaching sphere of the 2-handle, only cusping instead of going through the handle. Notice that the meridian curve goes between the 2 sides labelled a_1 on the square and the longitudinal curve goes between the sides identified as a_2.

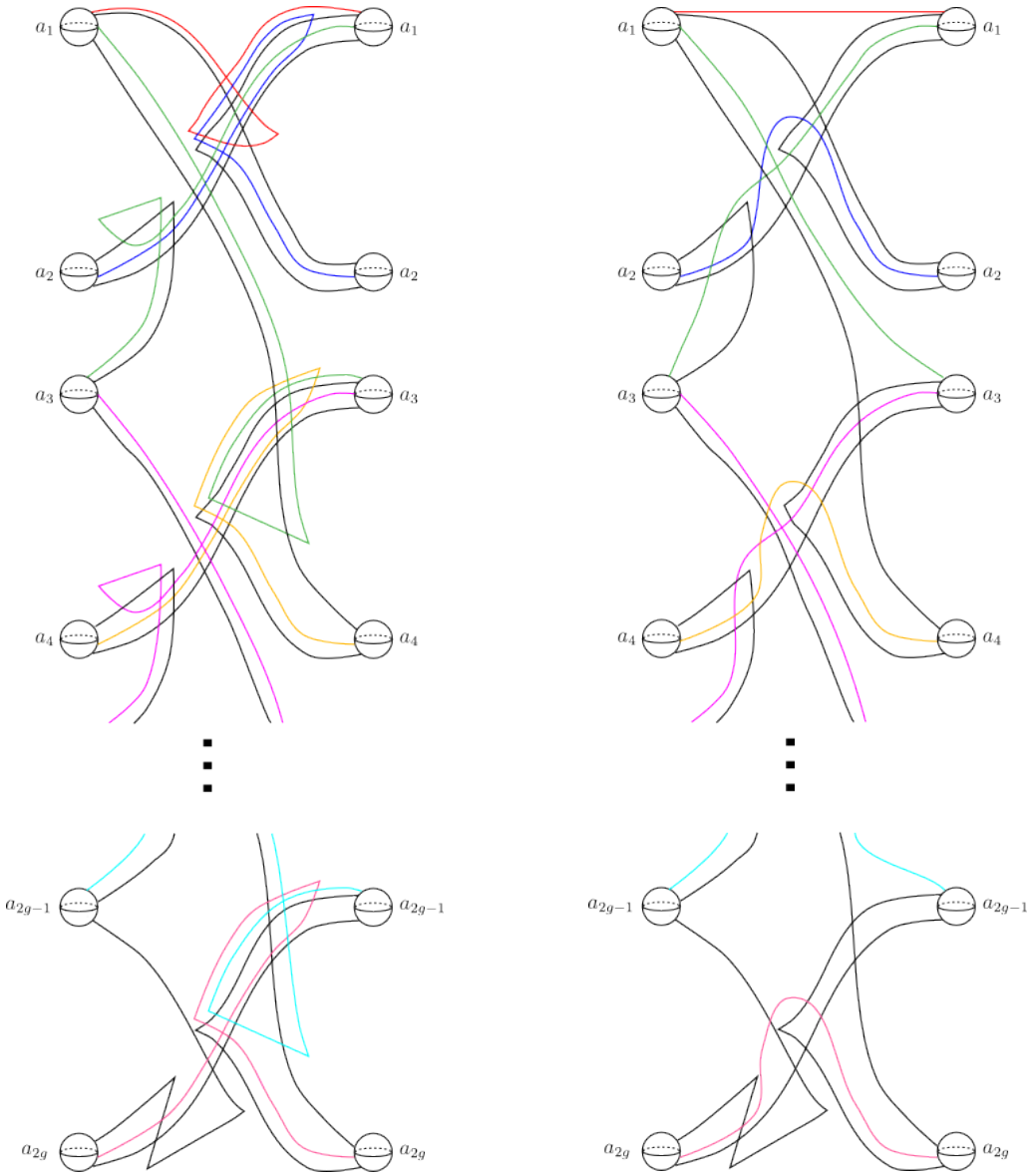

(A) $T^*\Sigma_g$ with $2g$ Lagrangian disks (B) A simplified version of this diagram

FIGURE 9. The Legendrian lifts of the curves in Σ_g

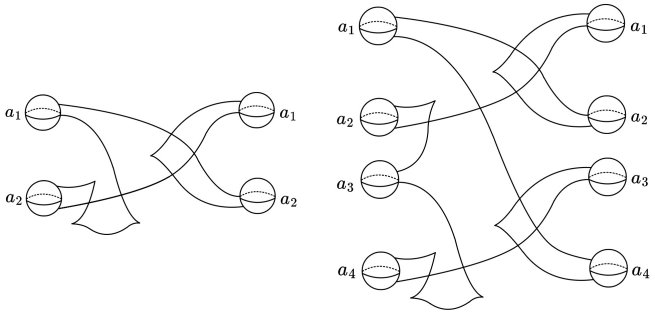

FIGURE 10. The Gompf standard handlebody diagrams of $T^*\Sigma_1$ (left) and $T^*\Sigma_2$

Now, consider the skeleton for the genus 2 case, as depicted in Figure 13. If we consider the fundamental polygon for this surface, then there is still a meridian curve connecting the two a_1 edges,

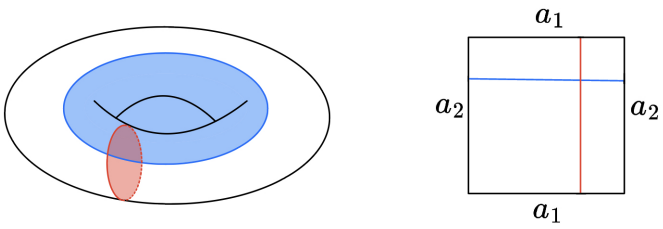

FIGURE 11. Left: Σ_1 with 2 Lagrangian disks. Right: The boundary curves on the representative polygon.

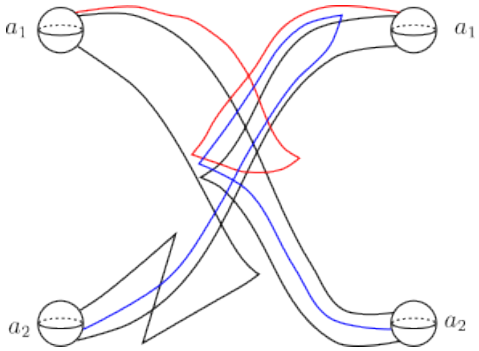

FIGURE 12. The handlebody diagram of $T^*\Sigma_1$ with lifts of the boundary curves.

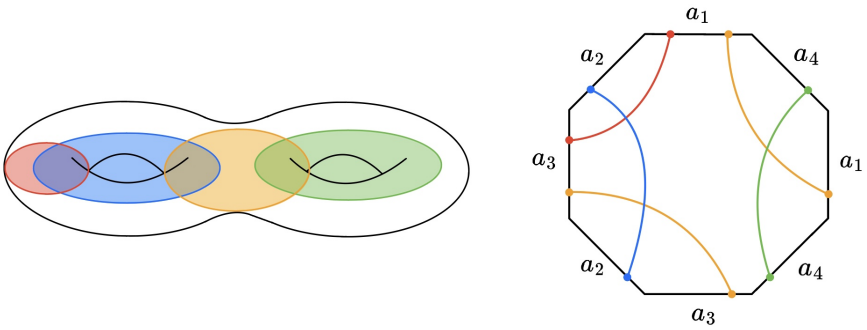

FIGURE 13. Left: Σ_2 with 4 Lagrangian disks. Right: The boundary curves on the representative polygon.

a longitudinal curve connecting the two a_2 edges, and another longitudinal curve connecting the two a_4 edges. Moreover, we now have another boundary curve which is the connect sum of the two meridians connecting the a_1 and a_3 respectively. Thus, on the 8-gon representing Σ_2, the curves bounding the disks appear as in Figure 14. Again, we can take Legendrian lifts of the boundary curves to the handlebody diagram of $T^*\Sigma_2$.

To generalize this to the case for arbitrary genus g, we will repeat the procedure of first considering how the disks forming the skeleton appear on Σ_g, then represent the boundary curves of the disks on the representative polygon of Σ_g, and then draw in the lifts of these curves to the Gompf diagram of $T^*\Sigma_g$.

First, consider Σ_g with the Lagrangian disks attached, as in Figure 15. A curve connecting any two sides labelled a_{2k-1} will correspond to a meridian, whereas the curves connecting any two sides labelled a_{2k} are longitudes (where $1 \leq k \leq g$). Considering the $4g$-gon representing Σ_g, we will have a meridian curve between the 2 edges labelled a_1, a curve connecting every pair of edges labelled a_{2k} $(1 \leq k \leq g-1)$, and connect sums of the respective curves connecting the edges labelled a_{2k-1}, a_{2k+2} such that the resulting connect sum intersects the a_{2k}, a_{2k+2} longitudes exactly once. Thus, the curves drawn on the $4g$-gon are as in Figure 16.

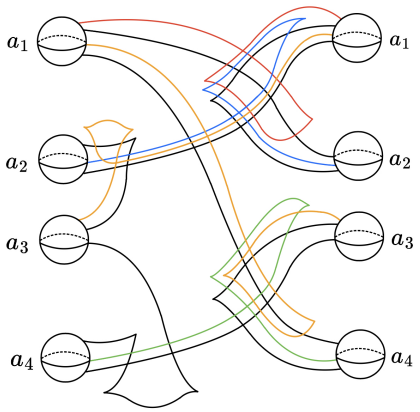

FIGURE 14. The handlebody diagram of $T^*\Sigma_2$ with lifts of the boundary curves

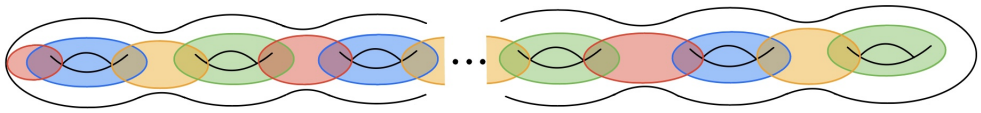

FIGURE 15. $T^*\Sigma_g$ with $4g$ embedded Lagrangian disks.

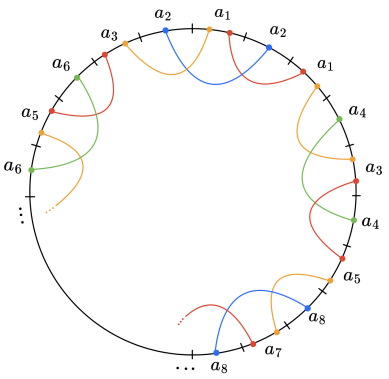

FIGURE 16. The representative polygon of Σ_g with boundary curves of the disks

Notably, to get from the polygonal representation of Σ_g to that of Σ_{g+1} with the corresponding set of Lagrangian disks attached, we simply add in the sequence of edges described above.

The two curves corresponding to the boundaries of the two new disks will be a connect sum of the old curves connecting the sides labelled $a_{2(g+1)-1}, a_{2(g+1)-3}$, and a longitudinal curve connecting the pair of edges labelled $a_{2(g+1)}$. In particular, the new curves will not interfere with any of the curves connecting any sides labelled a_k for $1 \leq k \leq 2(g+1)-3$. To draw the lifts of these curves in the Gompf diagram for $T^*\Sigma_g$, we follow a curve coming out of an edge, which corresponds to the 1-handle the curve comes out of on the Gompf diagram. Then, continue drawing the curve by following the attaching sphere of the 2-handle of $T^*\Sigma_g$, cusping if we reach the attaching sphere of a 1-handle that this curve does not enter.

Following this procedure, we obtain Figure 9a, which was the desired handlebody diagram. Figure 9b can be obtained by simplifying through Reidemeister moves. □

By a sequence of standard Legendrian Reidemeister moves, we can simplify this handlebody diagram to the one below. We will work with this simplified diagram for the remainder of this paper.

3.2. **Technical lemmas for manipulating Weinstein Kirby diagrams.** We now present a number of technical lemmas that allow for easier manipulations of Weinstein handlebody diagrams. The first of these lemmas establishes conditions under which cusps and crossings can be pushed past fixed cusps.

Lemma 3.2. *The pair of Weinstein handlebody diagrams in Figure 17 are equivalent, where the box in the Weinstein handlebody diagram below represents an ordered sequence of crossing, left cusps, and right cusps, with ordering indicated by the arrow.*

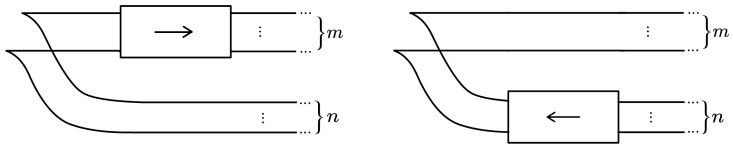

FIGURE 17. The equivalent diagrams of Lemma 3.2

Proof. It suffices to show that individual crossings, left cusps, and right cusps can be moved past fixed cusps.

Any strands cusping above a given crossing or cusp can be moved behind the crossing or cusp by Reidemeister 3 or 2 moves respectively. For example, when pushing a crossing past a set of cusps, the strands cusping above the crossing are moved behind the crossing by Reidemeister 3 moves (Figure 18).

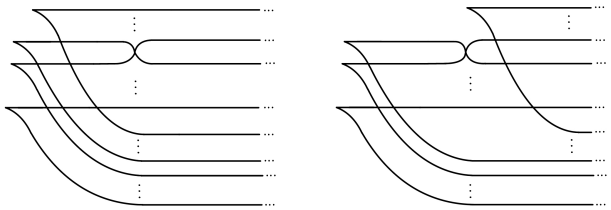

FIGURE 18. Pushing a crossing past a set of cusps

Thus, we need only consider the strands lying below the crossing. Working with this simplified diagram and disregarding the upper strands, a Reidemeister 2 move pulls in the uppermost cusp. The cusp is pushed out again via another Reidemeister 2 move, and a Reidemeister 3 move finally moves the crossing past the cusp, as shown in the sequence of diagrams in Figure 19.

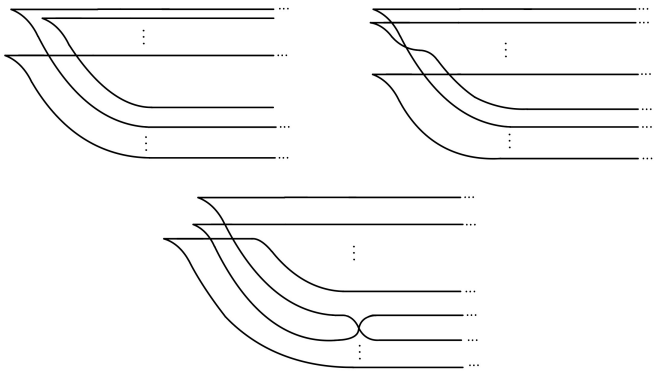

FIGURE 19. Moving the crossing below a cusp

Left cusps can also be pushed past existing cusps. The sequence of moves depends on whether the left cusp is fully "external" and hence disjoint from the fixed cusps it is to be pushed past, or if it "interlocks" one of the fixed cusps.

In the first case, depicted in Figure 20, the red cusp is moved past the two black cusps. (Note that any strands cusping above the red cusp are omitted in the diagram, because they can be moved out of the way by a Reidemeister 2 move.) To do so, we introduce a new crossing via a Reidemeister 1 move, and consecutive Reidemeister 2 moves push the red cusp through the fixed black cusp.

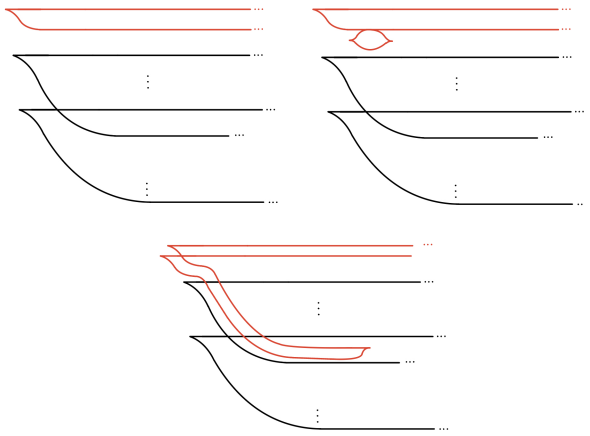

FIGURE 20. Pushing left cusps past existing cusps

A similar sequence of Reidemeister moves can be applied if the cusp to be moved interlocks with one of the fixed cusps, i.e., is located over one of the strands making up the fixed cusps. Namely, we have the series of equivalences in Figure 21. Here, two new cusps and crossings are introduced

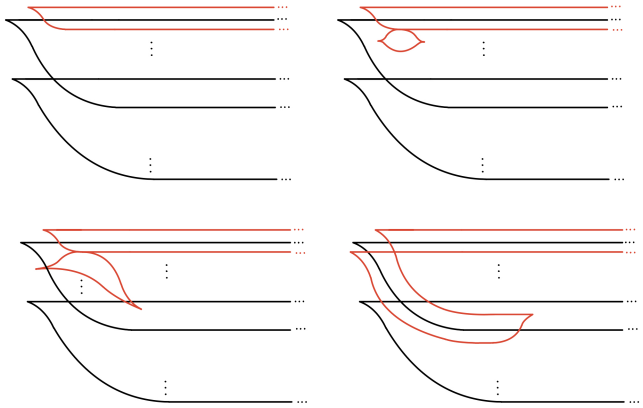

FIGURE 21. Moving a cusp which "interlocks" with a fixed cusp

using a Reidemeister 1 move. The new cusps are then both pulled through the black strand using Reidemeister 2 moves, and a Reidemeister 3 move yields the third equivalence.

Likewise, we can push right cusps past pairs of fixed cusps. In Figure 22, the red right cusp is pushed through the black cusps using two Reidemeister 2 moves.

We can also move a right cusp which "interlocks" with a black cusp. In Figure 23, the uppermost black cusp is pulled in via a Reidemeister 2 move, and the remaining steps are exactly as before.

This exhausts all possible cases. Thus, all crossings, left cusps, and right cusps can be pushed past any number of fixed cusps in this manner. Now by sequentially moving each crossing or cusp past the pair of fixed cusps, the entire fixed sequence of ordered cusps and crossings can be moved. □

Lemma 3.2 allows us to define a generalization of the Reidemeister 1 move.

Corollary 3.3. *The two handlebody diagrams in Figure 24 are equivalent, where the box once again represents an ordered sequence of left cusps, right cusps, and crossings.*

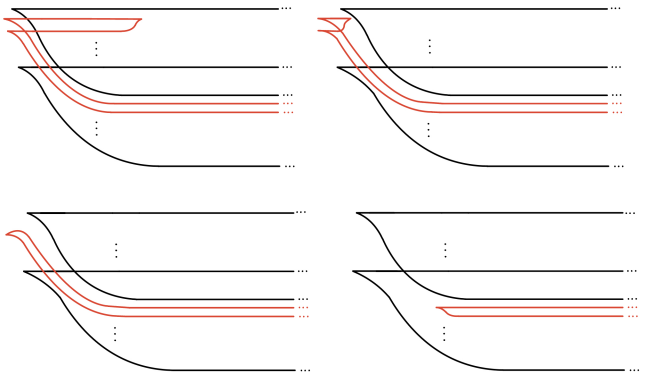

FIGURE 22. Pushing an "internal" right cusp through the black cusps

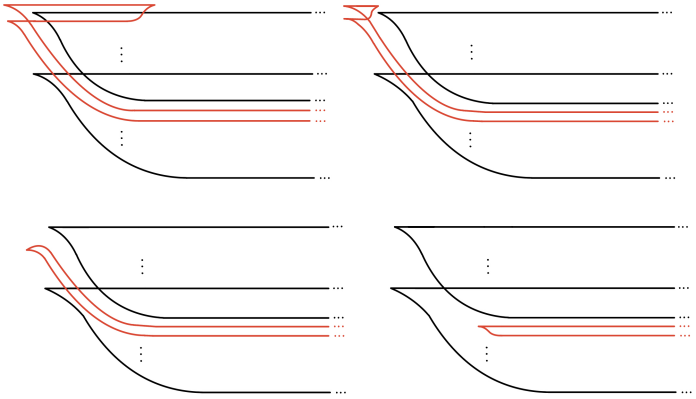

FIGURE 23. Pushing an "interlocking" right cusp through the black cusps

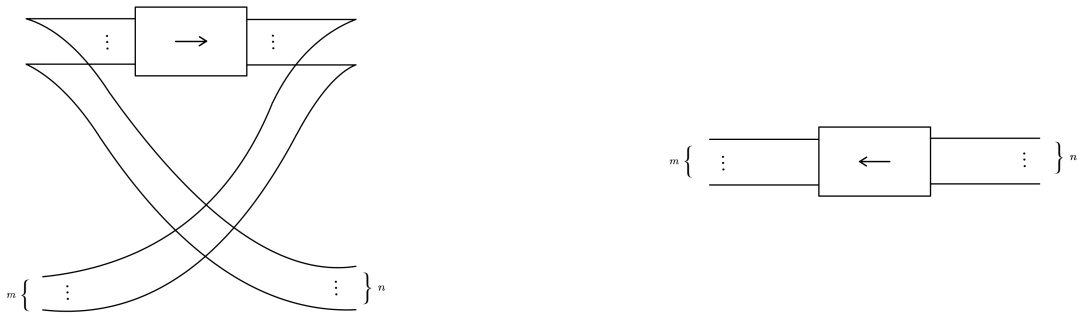

FIGURE 24. The equivalent diagrams of Corollary 3.3

Proof. Using Lemma 3.2, we have the equivalence in Figure 25. In particular, to move the box through the main crossing in the middle, we can simply use a combination of Reidemeister 3 (for crossings) and Reidemeister 2 (for left and right cusps) moves.

Now, starting at the lowest strand (highlighted in red), we perform a Reidemeister 3 move and two Reidemeister 2 moves to bring the lowest twist under the other strands, as depicted in Figure 26. The red crossing is untwisted using a Reidemeister 1 move, so that the red strand now simply lies at the bottom of the diagram.

We now repeat the same procedure, as shown in Figure 27, to untwist all the strands. A final Reidemeister 1 move untwists the uppermost crossing, giving us the desired diagram. □

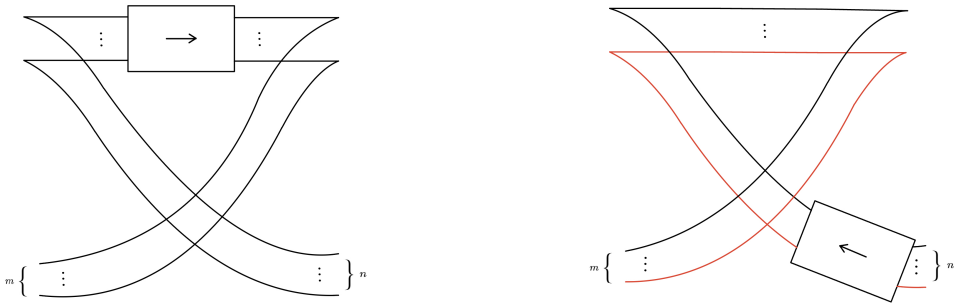

FIGURE 25. Sliding a box out of two overlapping Reidemeister 1 strands

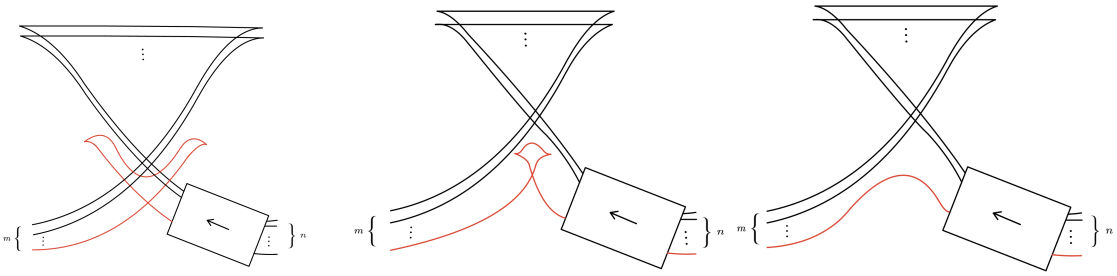

FIGURE 26. Moving the lowest (red) strand down

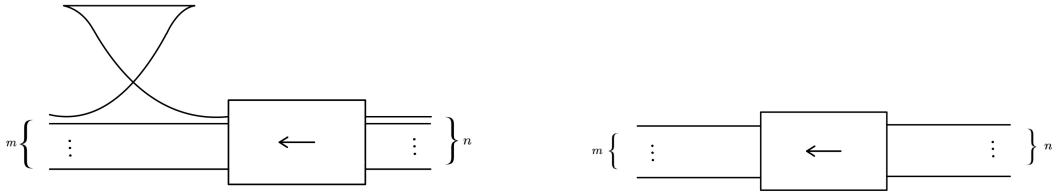

FIGURE 27. Untwisting all the strands

Both Lemma 3.2 and Corollary 3.3 hold in slightly greater generality. Given a group of (not necessarily ordered) crossings, left cusps, and right cusps, this group can always be ordered by smoothly deforming the diagram. After this deformation, the lemma and corollary can be applied.

We prove another technical lemma on the equivalence of certain sections of handlebody diagrams.

Lemma 3.4. *The pair of Weinstein handlebody diagrams in Figure 28 are equivalent.*

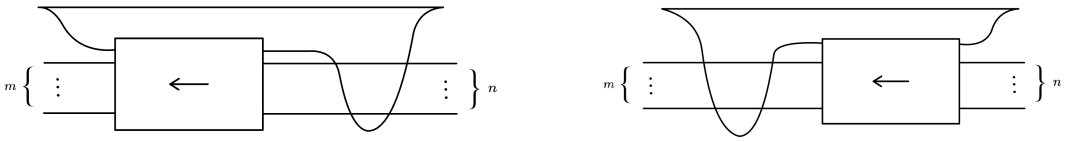

FIGURE 28. The equivalent diagrams of Lemma 3.4

Proof. We first perform a Reidemeister 1 move in the bottom right and apply two consecutive Reidemeister 3 moves to the resulting crossing. Since the box consists of crossings and cusps, we can move a strand through the entire box with Reidemeister 2 and 3 moves, as shown in Figure 29.

This creates a crossing on the left side of the diagram, which can be untwisted using a Reidemeister 1 move. We now perform another Reidemeister 1 move to create a new crossing on the top right of the diagram. This brings us to the diagrams shown in Figure 30. Now we can once again move one of the strands through the box of cusps and crossings using Reidemeister 2 and 3 moves. The resulting

FIGURE 29. Moving a strand through the box

FIGURE 30. Introducing a new crossing on the top right

crossing on the bottom left of the diagram can again be untwisted with a Reidemeister 1 move, which gives us the desired equivalence of diagrams in Figure 31. □

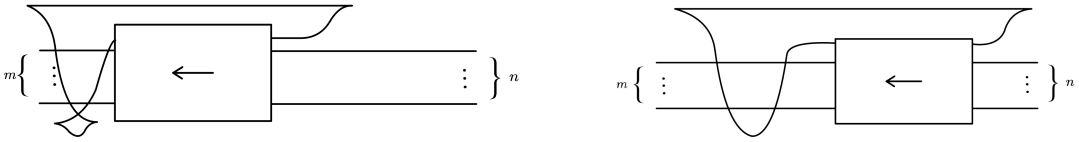

FIGURE 31. Moving the box through and untwisting

Corollary 3.5. *The local parts of the Weinstein handlebody diagrams in Figure 32 are equivalent, where the box represents the* $(2, 2n)$*-torus knot. In other words, we can "mirror" across a torus knot.*

FIGURE 32. The equivalent diagrams of Corollary 3.5

Proof. This proof is fully presented in Figure 33. In particular, we begin by performing a Reidemeister 1 move in the bottom right, as in Figure 33a.

Next, a series of Reidemeister 3 moves allows us to move a strand, namely the left half of the crossing in Figure 33a, through the crossings in the middle, as shown in Figure 33b. Note that geometrically, this segment of the attaching sphere lies behind the rest of the objects in the diagram. After a Reidemeister 2 and 1 move on the left side, we then perform a Reidemeister 1 move on the right side, as in Figure 33c.

Similarly to before, we perform a series of Reidemeister 3 to get to Figure 33d. This moves the strand across the crossings in the middle, and we can untwist it with a Reidemeister 1 move. If we isolate the two rightmost crossings in the block, as in Figure 33f, we can see that we can apply Lemma 3.4 to move these over to the left.

In fact, we can apply this n times to end up with all of these on the left side, which gives us Figure 33g. Note that this diagram is in fact a reflection of Figure 33e. Hence reflections of the same steps from before implies that we get Figure 33h, as desired. □

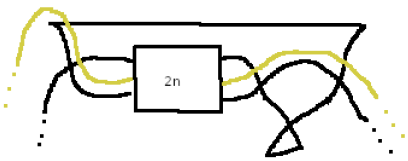

(A) Adding a crossing in the bottom right

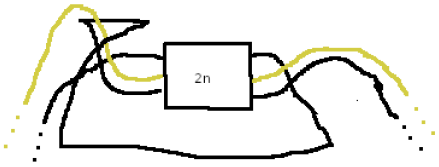

(B) Moving the strand through the torus knot

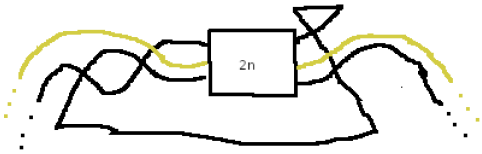

(C) Untangling the left side and twisting the right side

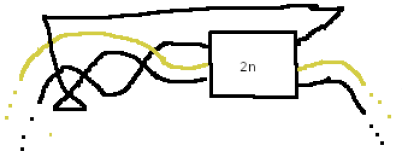

(D) Moving the strand through the torus knot again

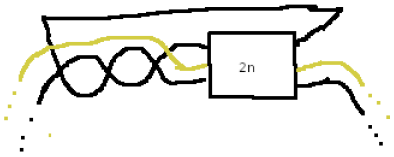

(E) A Reidemeister 1 move

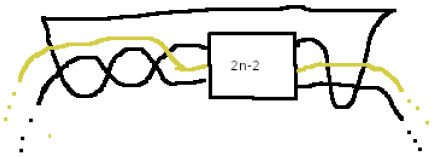

(F) Expanding some crossings of the torus knot

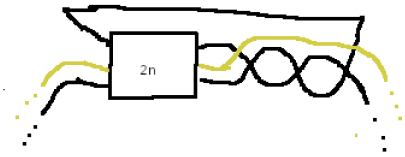

(G) Moving the torus knot to the left side

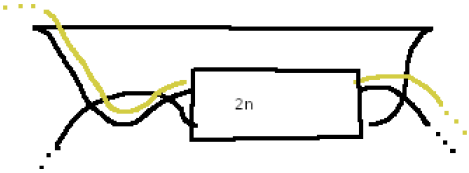

(H) Mimicking the previous steps

FIGURE 33

3.3. **The main theorem.** With these lemmas, we are almost ready to prove our main theorem, which states that the diagram from Proposition 3.1 actually reduces to a $(2, n)$-torus knot. To begin, we prove a result relating handle cancellations in one important case, namely in a version of the diagram from Proposition 3.1. This will help us inductively prove our main theorem.

Lemma 3.6. *Given a diagram similar to the Gompf diagram for a genus g surface, only with a torus knot on the top, we can cancel two handles as shown in Figure 34 by simply adding two crossings to*

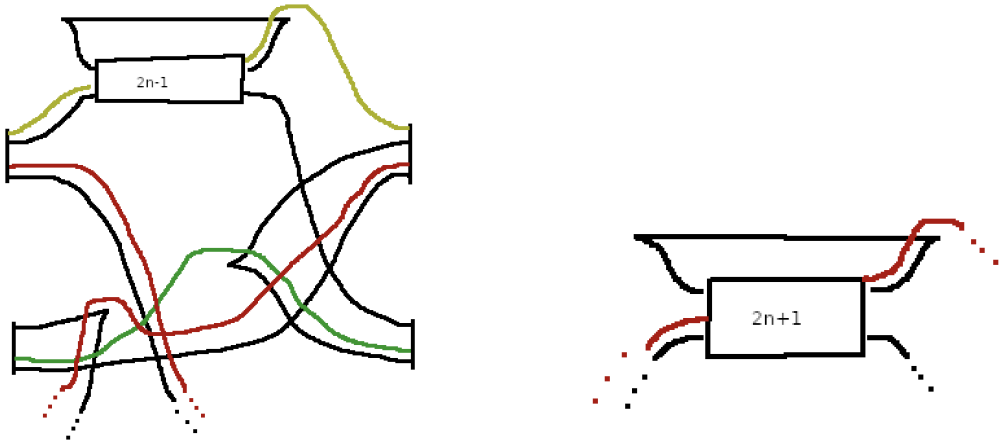

FIGURE 34. The equivalent diagrams of Lemma 3.6

the torus knot. Naturally, we also have that the diagrams in Figure 35 are equivalent.

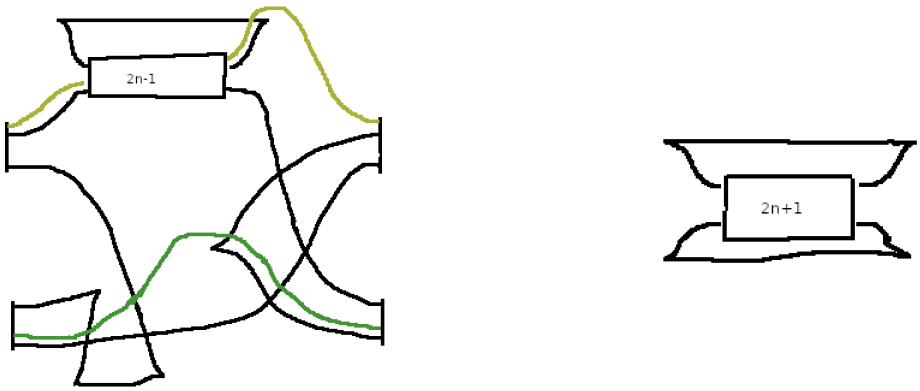

FIGURE 35. A special case of Lemma 3.6

Proof. We begin by sliding thrice over the yellow handle, then cancelling it with the 1-handle. This leaves us with the first diagram in Figure 36. We now have three interlocking cusps on the left side. Then we can apply a series of Reidemeister 2 and 3 moves to move the innermost cusp past all the

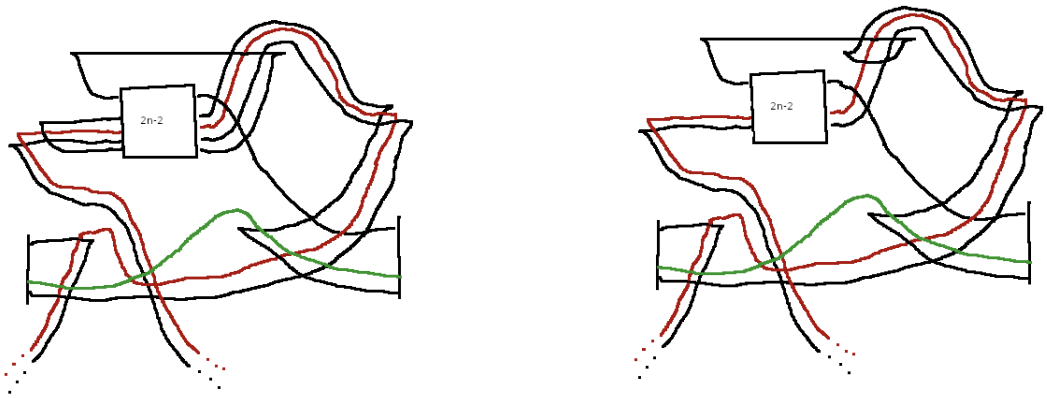

FIGURE 36. A triple handle slide

crossings. Then by redrawing and sliding over the green handle, we get Figure 37.

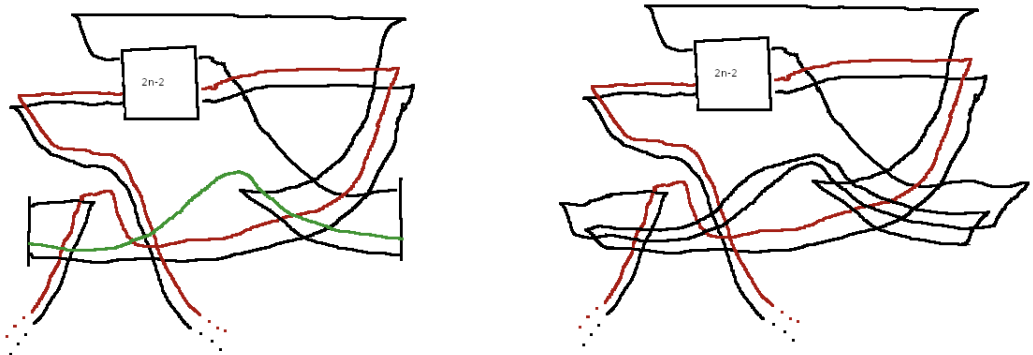

FIGURE 37. Handle sliding over the green handle

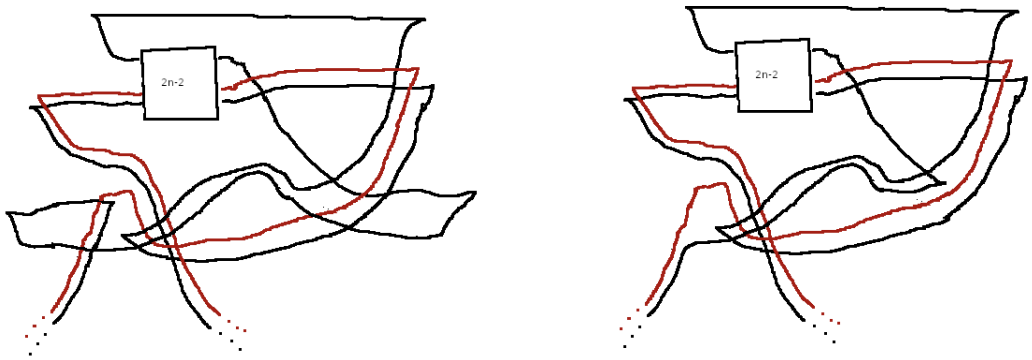

FIGURE 38. Simplifying the previous diagrams

Now we use a sequence of Reidemeister 2 and 3 moves followed by a Reidemeister 1 move on the right, and a similar sequence of Reidemeister 2 and 3 moves on the left. Pulling the leftmost and rightmost cusps in gets us Figure 38.

With a sequence of Reidemeister 3 moves, we move the upper strand of the bottom-most cusp across all of the crossings in the middle. Additionally, we do two Reidemeister 2 moves, sending the innermost right cusp upwards on the right side. Applying Lemma 3.2 on the right, we get Figure 39.

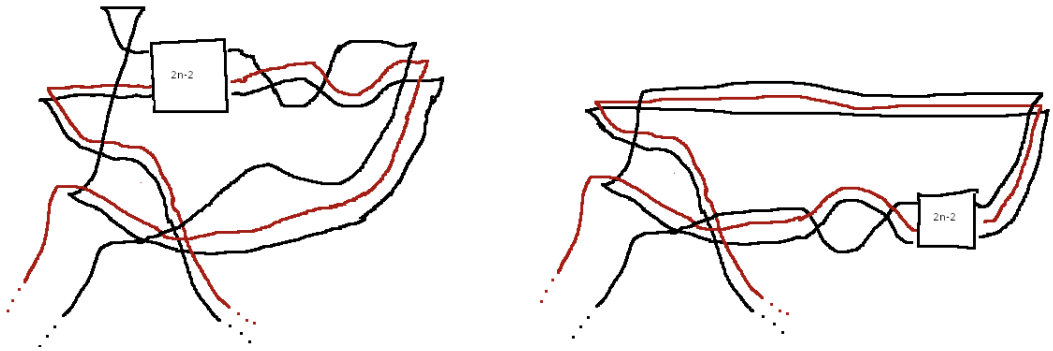

FIGURE 39. Moving the two internal cusps and untwisting the top

Now, on the top left, we do Reidemeister 2 and 3 moves to move the red and black cusps inside. Then we apply a sequence of Reidemeister 3 moves to move the red and black strands past all of the crossings in the middle. This gives two interlocking Reidemeister 1-type strands on the right side, as shown in Figure 40a. To get Figure 40b, we simply use Reidemeister 2 and 3 moves to move the cusps

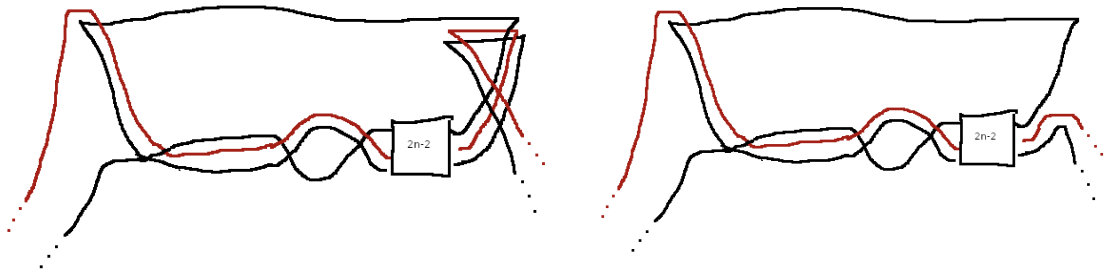

(A) Moving the left cusps through the center (B) Untwisting with Reidemeister 1 moves

FIGURE 40

on the right out, followed by two Reidemeister 1 moves to untwist.

Finally, applying Corollary 3.5 gives us the desired diagram in Figure 34. The diagrams in Figure 35 are of course a special case of this. □

With this, we are finally ready to prove our main theorem.

Theorem 3.7. *The 4-manifold obtained by attaching $2g$ Lagrangian disks to the cotangent bundle of the genus g surface is equivalent to the 4-manifold obtained by attaching a Weinstein 2-handle to a Weinstein 0-handle along a $(2, 2g+1)$-torus knot. Namely, the Weinstein handlebody diagrams in Figure 41 are equivalent.*

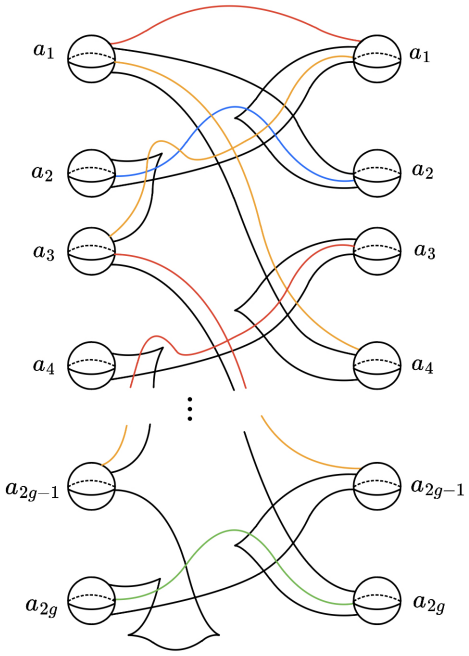

(A) $T^*\Sigma_g$ with $2g$ embedded Lagrangian disks

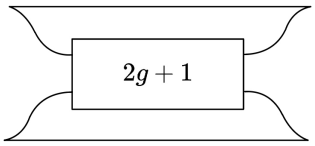

(B) The Legendrian $(2, 2g+1)$-torus knot

FIGURE 41

Proof. We begin by applying a Reidemeister I and II move to the top of the handlebody diagram in Figure 41a. This allows us to apply Lemma 3.6, which cancels the top two 2-handles and simplifies the diagram as shown:

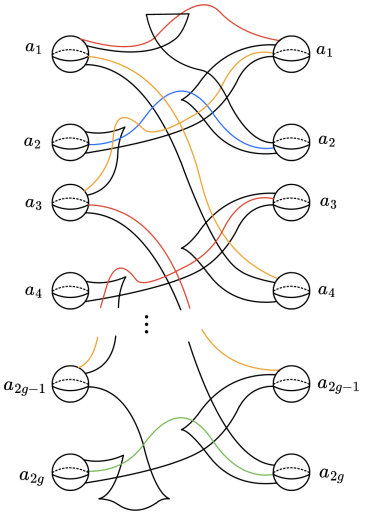

(A) Creating a twist at the top of the diagram

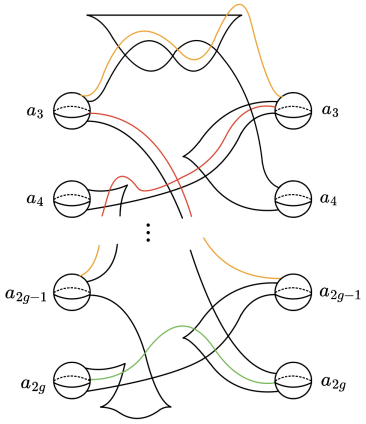

(B) Applying Lemma 3.6

FIGURE 42

The top of diagram Figure 42b is similar to the $(2,3)$-torus knot, so we may again apply Lemma 3.6. Continuing in this way, we can apply Lemma 3.6 a total of $g-1$ times. With each application, two crossings are added to the torus knot at the top of the diagram, and a pair of 1-handles is cancelled with a pair of 2-handles. The resulting diagram is precisely the diagram appearing in Figure 35, so a final application of Lemma 3.6 simplifies our diagram as below.

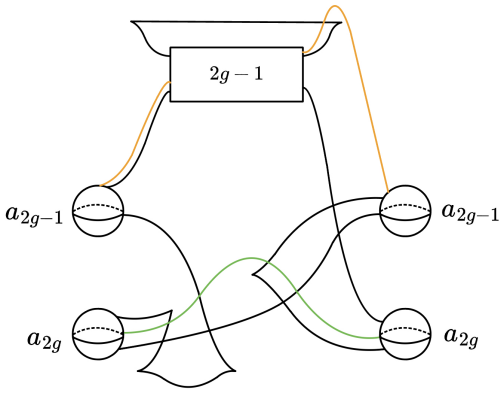

(A) Repeating the above process $g-1$ times

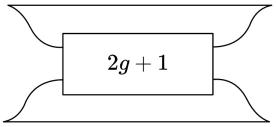

(B) Applying Lemma 3.6 one last time

FIGURE 43

As claimed, Figure 43b is the Weinstein handlebody diagram for the symplectic 4-manifold constructed by attaching a Weinstein 2-handle to a 0-handle along a Legendrian $(2, 2g+1)$ torus knot. □

REFERENCES

[1] Bahar Acu, Orsola Capovilla-Searle, Agnès Gadbled, Aleksandra Marinković, Emmy Murphy, Laura Starkston, and Angela Wu. Weinstein handlebodies for complements of smoothed toric divisors, 2020.

[2] Robert E. Gompf. Handlebody construction of Stein surfaces. *Ann. of Math. (2)*, 148(2):619–693, 1998.

[3] Robert E. Gompf and András I. Stipsicz. 4-*manifolds and Kirby calculus*, volume 20 of *Graduate Studies in Mathematics*. American Mathematical Society, Providence, RI, 1999.

[4] David Nadler. Arboreal singularities. *Geom. Topol.*, 21(2):1231–1274, 2017.

[5] Alan Weinstein. Contact surgery and symplectic handlebodies. *Hokkaido Math. J.*, 20(2):241–251, 1991.